*This work was supported by the Advanced Projects Agency under Army Contract No. DA-31-124-ARO-(D)-14.

†Present address: Department of Physics, Louisiana Polytechnic Institute, Ruston, Louisiana.

‡Present address: Department of Chemistry, Brookhaven National Laboratory, Upton, N. Y.

[1]W. L. Clinton, J. Nakhleh, and F. Wunderlich, Phys. Rev. __177__, 1 (1969); (paper I);

W. L. Clinton, A. J. Galli, and L. J. Massa, Phys. Rev. __177__, 7 (1969); (paper II);

W. L. Clinton, G. A. Henderson, and J. V. Prestia, Phys. Rev. __177__, 13 (1969); (paper III);

W. L. Clinton and G. B. Lamers, Phys. Rev. __177__, 19 (1969) (paper IV, preceding paper).

[2]Several authors [see W. Byers Brown, J. Chem. Phys. __44__, 567 (1966), and references therein] have recently explored the use of empirical constraints in conjunction with Hartree-Fock calculations. Mukerji and M. Karplus [J. Chem. Phys. __38__, 44 (1963)], for example, adjust the Hartree-Fock wave function directly in the case of the $F-H$ molecule in order to reproduce the experimental dipole moment and field gradient at the proton.

[3]J. O. Hirschfelder, J. Chem. Phys. __33__, 1462 (1960).

[4]R. McWeeny, Rev. Mod. Phys. __32__, 335 (1960). See also paper II in the present series.

[5]For reasons discussed in paper IV, these constraints have been symmetrized.

[6]The actual mechanics of extracting a normalized eigenvector from an idempotent $\underline{P}_i$ with $\mathrm{Tr}\underline{P}_i < 1$ is simple. By virtue of the factorization $\underline{P}_i = \underline{C}_i \underline{C}_i{}^\dagger$, every column of $\underline{P}_i$ is proportional to $\underline{C}_i$. It is only necessary, then, to renormalize a given column of $\underline{P}_i$. On the other hand, one may choose to formulate the eigenvalue problem such that $\underline{P}^2 = \underline{P}$ and $\mathrm{Tr}\underline{P} = n < m$. This implies that $\underline{P} = \underline{C}\,\underline{C}^\dagger$ where $\underline{C}$ is a rectangular matrix $(m \times n)$ containing n eigenvectors. This approach has the advantage of requiring the determination of fewer density matrices, but suffers in that an independent scheme for extracting the n eigenvectors is necessary.

[7]H. M. James, J. Chem. Phys. __3__, 9 (1935).

[8]Here we work in terms of a "full" N-electron matrix defined as $\underline{P} = \underline{C}\,\underline{C}^\dagger$ where $\underline{C}$ is $m \times N/2$ and contains all $N/2$ eigenvectors. (See Ref. 6.)

[9]Here again symmetrization is understood. For brevity, we do not display it.

[10]Figure 3 is for a Clementi function; E. Clementi, J. Chem. Phys. __38__, 996 (1963). Figure 4 is the local energy of the 12-function exponential-polynomial basis of Roothaan, Sachs, and Weiss, Rev. Mod. Phys. __32__, 186 (1960).

[11]A. A. Frost et al., Rev. Mod. Phys. __32__, 313 (1960).

[12]C. C. J. Roothaan and A. Weiss, Rev. Mod. Phys. __32__, 194 (1960).

[13]W. Bingel, private communication.

[14]For a general discussion of orthogonal operators, see U. Fano, Rev. Mod. Phys. __29__, 74, (1957).

[15]D. R. Bates et al., Phil. Trans. Roy. Soc. London __246__, 215 (1953).

Many-Body Approach to Hyperfine Interaction in Atomic Nitrogen*

N. C. Dutta, C. Matsubara, R. T. Pu, and T. P. Das
Department of Physics, University of California, Riverside, California
(Received 12 July 1968)

The Brueckner-Goldstone many-body perturbation theory has been applied to calculate the hyperfine constant a of atomic nitrogen in its ground state $^4S_{3/2}$. The exchange core-polarization diagrams lead to contributions of $-49.710\,72$ and $55.418\,82$ Mc/sec from the $1s$ and $2s$ states, respectively, adding to a total of $5.708\,10$ Mc/sec. Higher-order diagrams characterizing mainly correlation effects produce an additional contribution of $4.780\,22$ Mc/sec. The total theoretical result 10.49 ± 0.15 Mc/sec is in excellent agreement with the experimental value of $10.45 \pm 0.000\,07$ Mc/sec. The major correlation effect arises from the interaction between the valence electrons and core s electrons, the effect of the $2s$ being the dominant one. It is found that a knowledge of the wave function up to second order is adequate for a sufficiently accurate evaluation of the hfs constant. The trends in the contribution from various physical effects observed by an analysis of pertinent diagrams are expected to be helpful in simplifying the analysis of more complex atoms.

I. INTRODUCTION

The Brueckner-Goldstone (BG) linked-cluster perturbation approach[1] to many-body theory has been applied successfully by Kelly[2,3] to the atomic systems beryllium and oxygen. The method was shown to yield excellent results for correlation energy, polarizabilities, and shielding factor. The BG theory was also used recently for calculation of the ground-state properties of atomic lithium by Chang, Pu, and Das.[4,5] In particular, Chang et al.[4] utilized this approach for the first time in a calculation of the hyperfine structure (hfs) constant of lithium atom ^2S and obtained good

agreement with experiment. The same method was subsequently used in hfs calculations of lithium ^2P state[6] and helium ^3S state, [7] again yielding good results in both cases. From the applications to these simpler atomic systems, much experience and physical insight have been gained, and it is of interest to test the applicability of the many-body approach for hfs of more complex atoms. In this paper we report the results of our investigation on the BG perturbation approach to a hfs calculation for the ground state $^4S_{3/2}$ of atomic nitrogen.

The BG theory, which gives both the energy and the wave function of a many-fermion system, embodies certain features which are especially desirable in the hfs calculation for complex atoms. We enumerate them here briefly. These features will be discussed further in Sec. V where our result will be compared with those from other methods.

First, in the BG perturbation method, the wave function of the system, to each order, is an eigenfunction[3,4] of $\vec{S}^2$, as demanded by the commutation properties of the atomic Hamiltonian. This is in contrast to the unrestricted Hartree-Fock (UHF) method, [8-11] where the wave function in general is not an eigenfunction of $\vec{S}^2$.

Secondly, in the BG theory, once the basis wave functions are determined by the choice of the one-particle potential V, one has a complete set of states. In comparison, one of the most used variational methods for calculating many-body atomic wave functions is the configuration interaction (CI) approach, [12,13] which involves a linear combination of determinantal functions, each representing a particular configuration of the electrons in the atom. Although, unlike the UHF method, the wave function in a CI approach is also an eigenfunction of $\vec{S}^2$, it suffers from the difficulty that in practice one can only deal with a finite number of configurations, and thus an incomplete basis set. Also the choice of the trial wave function is rather arbitrary. These difficulties can become really severe in heavy atoms if one is to obtain a meaningful result.

Thirdly, in hfs calculation, one is interested in the difference between spin-up and spin-down electron densities at the nucleus. In both the UHF and CI approaches, one actually calculates the density for spin-up and spin-down electrons individually first and then subtracts. Since in general this density difference comes out to be 1 to 0.1% or even less of the individual spin densities, the hfs calculation in these methods involves the difference of large numbers, hence there is a problem of numerical accuracy. The problem becomes all the more acute in the case of heavier atoms since the hfs contributions from different s shells often have opposite signs and the net hfs value is again the small difference of these values. This is the case in our present nitrogen calculation and can be even more drastic in other situations. [14,15]

On the other hand, in the BG perturbation theory one may make formal cancellations prior to calculation. [2-4] Thus one deals directly with terms corresponding to the spin-density difference in common with other perturbation methods such as the exchange perturbation[16] (EP) or the moment perturbation[17] (MP) methods. In fact, the EP or MP method corresponds to the first-order contribution in the BG method.

Each term in the BG perturbation expansion can be represented by a Feynman-type diagram. In addition to facilitating the enumeration of terms, the diagrammatic approach enables one to identify the contributing terms with certain physical processes. This is perhaps the most attractive feature of the BG method since it enables considerable physical insight and an assessment of the relative importance of various contributions to the hfs from different physical processes, such as the exchange core-polarization, inter- and intra-shell correlations, self-consistency, and mutual polarization of orbitals. This information enables one to better appreciate the physical significance of various other methods, [9,12,17-19] that have been used for calculating hfs.

In Sec. II, a short review of the important points of BG theory will be presented. Section III will deal with some relevant details of procedure such as the choice of the single-particle potential V, the calculation of bound and excited-state wave functions, and the relation between the hyperfine constant a and hyperfine matrix elements. Section IV will enumerate the various hyperfine diagrams and their contributions to a. Section V will discuss the significance of the values of various diagrams and finally a comparison of our final result with experiment[20] and other theoretical values[8,12,18,19,21] of a.

II. REVIEW OF BRUECKNER-GOLDSTONE THEORY

Since the features of BG theory pertinent to atomic problems have been reviewed in several places earlier, [2-5] we shall not enter into a detailed description here. However, a brief resume of the most important points will be presented both for the sake of completeness and for a better understanding of the succeeding sections.

The exact nonrelativistic Hamiltonian for a neutral atom of N electrons is given by

$$\mathcal{H} = \sum_i T_i + \sum_{i>j} 1/r_{ij} , \qquad (1)$$

where T_i is the sum of the kinetic energy and the nuclear Coulomb potential operators for the ith electron

$$T_i = -\tfrac{1}{2} \nabla_i^2 - N/r_i . \qquad (2)$$

For convenience, atomic units are utilized in Eqs. (1) and (2) and throughout the rest of the paper. Equation (1) may be split into two parts, the unperturbed Hamiltonian

$$\mathcal{H}_0 = \sum_i T_i + \sum_i V_i \qquad (3)$$

which is the sum of the operator T_i and a one-body

potential operator V_i, and the perturbation

$$\mathcal{H}' = \sum_{i>j} 1/r_{ij} - \sum_i V_i \ . \tag{4}$$

The single-particle potential V is chosen to be Hermitian and it generates a complete orthonormal set of single-particle states, which are solutions of

$$(T+V)\varphi_i = \epsilon_i \varphi_i \ . \tag{5}$$

The true ground-state wave function Ψ_0 satisfies the eigenvalue equation

$$\mathcal{H}\Psi_0 = E\Psi_0 \ , \tag{6}$$

and the "unperturbed" ground state of the atom satisfies

$$\mathcal{H}\Phi_0 = E_0\Phi_0, \quad E_0 = \sum_{i=1}^N \epsilon_i \ . \tag{7}$$

The wave function Φ_0 is a determinant formed out of the N solutions of (5) which are lowest in energy. The single-particle states occupied in Φ_0 are called unexcited states. The remaining single-particle states of the orthonormal set are called excited states. An occupied excited state is called a particle, and an unoccupied unexcited state a hole.

From the BG linked-cluster perturbation theory, the true ground-state wave function Ψ_0 is given by

$$\Psi_0 = \sum_{n=0}^\infty {}^L \left(\frac{1}{E_0 - \mathcal{H}_0} \mathcal{H}' \right)^n \Phi_0$$

$$= |0\rangle + |1\rangle + |2\rangle + \cdots + |n\rangle + \cdots \ . \tag{8}$$

and the true ground-state energy by

$$E = E_0 + \langle \Phi_0 | \mathcal{H}' | \Psi_0 \rangle, \tag{9}$$

where L means that only "linked" terms are to be included, and $|n\rangle$ represents the nth order perturbation expansion of the wave function. In the presence of an external field as in polarizability calculations,[2,3,5] one can include in $\mathcal{H}'$ the perturbation Hamiltonian due to the external field. Each term of the expansion in (8) is represented by a number of Feynman-like diagrams, drawn according to certain definite rules.[2] In this diagrammatic representation of perturbation terms, the perturbation interactions $1/r_{ij}$ and the single-particle potential V are represented by ---- and ---- ×, respectively. Particles and holes are drawn as solid lines directed, respectively, upward and downward, the time axis being considered directed upward. The first-order wave function $|1\rangle$ is then

the sum of the diagrams in Fig. 1. The minus sign in front of the diagram (1a) indicates the negative sign of V in the $\mathcal{H}'$; i,j are hole states and k,k' denote particle states.

As we shall see later, from the definition of the single-particle potential V we use, a great deal of cancellation can be made among the diagrams (1a), (1b), and (1c). For our hfs calculation, another great reduction of diagrams occurs because of spin-up and spin-down cancellation, leaving only the net diagrams that represent the true spin difference to be calculated. The diagram (1d) describes the true two-body correlation correction and represents the term

$$\frac{\varphi_k \varphi_{k'} \langle i\,(1)j\,(2) | 1/r_{12} | k(1)k'(2)\rangle}{\epsilon_i + \epsilon_j - \epsilon_k - \epsilon_{k'}} \ . \tag{10}$$

Figure (1d) can be divided into two cases, viz., intershell correlation and intra-shell correlations, depending on whether hole states i and j are occupied with electrons belonging to same or different shell. It may be emphasized that whereas Diagrams (1a), (1b), and (1c) can be made to cancel by a suitable choice of V, Diagram (1d) will always survive; it expresses in diagrammatic form the Brillouin theorem[22] for closed-shell systems.

Higher-order diagrams representing higher-order perturbation wave functions are built from these particle and hole lines linked by interaction vertices of $1/r_{ij}$ type or the single-particle potential V type. We illustrate a few important second-order diagrams in Fig. 2, which will enter into our hfs calculations.

(a)   (b)

(c)   (d)
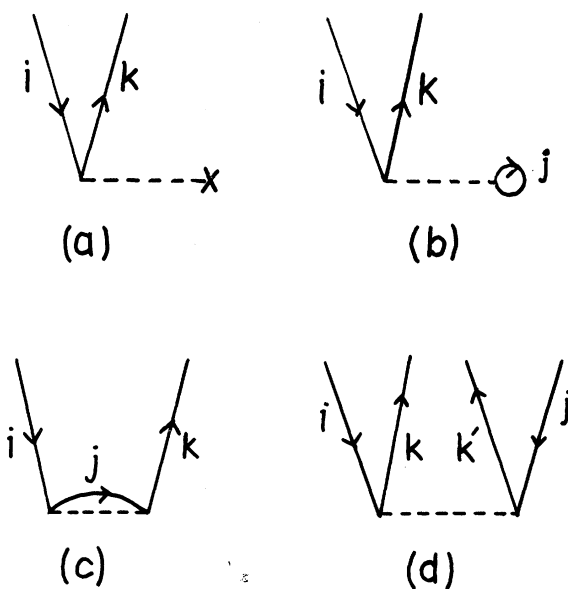
FIG. 1. First-order corrections to the unperturbed wave function Φ_0. (a) Interaction with the single-particle potential V. (b) Direct interaction with passive unexcited state j. (c) Exchange interaction with j. (d) Two-body correlation correction.

(a)   (b)   (c)
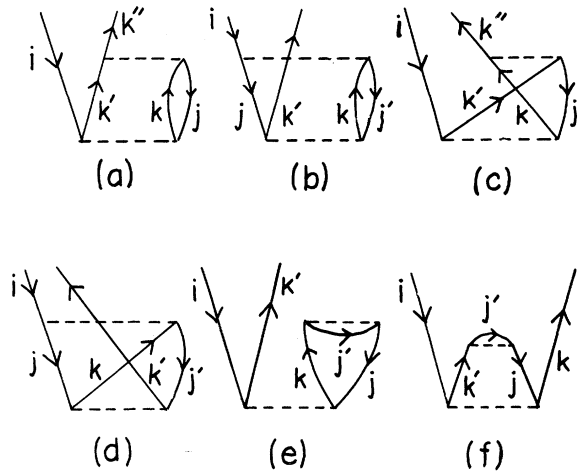
FIG. 2. Some second-order corrections to the unperturbed wave function Φ_0.

(d)   (e)   (f)

III. DESCRIPTION OF PROCEDURE

A. Single-Particle Potential

The choice of the single-particle potential V is at our disposal. It is to be chosen with a view towards making the BG series as easy and quickly convergent as possible. It has been found earlier[2-5] that it is desirable to use a potential such that the basis set generated resembles closely the bound and excited one-electron states of the N-electron system. We have chosen to work with what is designated by Kelly[2] as the V^{N-1} type potential. In this potential, the states are calculated in the field of $(N-1)$ electrons. Since we are concerned with the hfs of an open-shell system, it is important to specify that we shall utilize the restricted Hartree-Fock approximation (RHF) for V^{N-1}. At large distances, the V^{N-1} potential goes as $1/r$ and therefore the eigenspectrum has an infinite number of bound and continuum excited states. Owing to the orthogonality property of angular-momentum wave functions, one may choose different V for different partial waves. Our choice is thus: all s states are generated in the field of neutral nitrogen minus one of the $2s$ electrons, and similarly, all $p, d, f, \ldots$ states are calculated in the field of neutral nitrogen minus one $2p$ electron.

For our basis functions, we shall utilize the standard notation

$$\varphi_{nlm}(\vec{r}) = [P(nl; r)/r] Y_l^m(\theta, \phi) \chi_s(m_s).$$ (11)

The radial function $P(ns; r)$ for the s states is given by the solution of the equation

$$\left(\frac{d^2}{dr^2} + \frac{2N}{r} - \frac{4}{r} Y_0(1s^0, 1s^0; r) - \frac{2}{r} Y_0(2s^0, 2s^0; r) - \frac{6}{r} Y_0(2p^0, 2p^0; r)\right) P(ns; r)$$

$$+ \frac{2}{r} Y_0(1s^0; ns; r) P(1s^0; r) + \frac{1}{r} Y_1(2p^0, ns; r) P(2p^0; r) = \epsilon_{ns} P(ns; r)$$ (12)

where, in accordance with the usual Hartree notation,

$$Y_k(nl, n'l'; r) = r \int_0^\infty (r_<^k / r_>^{k+1}) P(nl; r') P(n'l'; r') dr'.$$ (13)

Correspondingly, the radial functions $P(np; r)$ and $P(nd; r)$ are obtained from the solution of the equations

$$\left(\frac{d^2}{dr^2} + \frac{2N}{r} - \frac{2}{r^2} - \frac{4}{r} Y_0(1s^0, 1s^0; r) - \frac{4}{r} Y_0(2s^0, 2s^0; r) - \frac{4}{r} Y_0(2p^0, 2p^0; r) + \frac{4}{25} Y_2(2p^0, 2p^0; r)\right) P(np; r)$$

$$+ \frac{2}{3r} Y_1(1s^0, np; r) P(1s^0; r) + \frac{2}{3r} Y_1(2s^0, np; r) P(2s^0; r) + \frac{16}{25r} Y_2(2p^0, np; r) P(2p^0; r) = \epsilon_{np} P(np; r)$$ (14)

$$\left(\frac{d^2}{dr^2} + \frac{2N}{r} - \frac{6}{r^2} - \frac{4}{r} Y_0(1s^0, 1s^0; r) - \frac{4}{r} Y_0(2s^0, 2s^0; r) - \frac{4}{r} Y_0(2p^0, 2p^0; r) + \frac{4}{105r} Y_2(2p^0, 2p^0; r)\right) P(nd; r)$$

$$+ \frac{2}{5} \left(\frac{1}{r} Y_2(1s^0, nd; r) P(1s^0; r) + \frac{1}{r} Y_2(2s^0, nd; r) P(2s^0; r) + \frac{0.88}{r} Y_1(2p^0, nd; r) + \frac{0.98}{r} Y_3(2p^0, nd; r) P(2p^0; r)\right)$$

$$= \epsilon_{nd} P(nd; r).$$ (15)

Here, $1s^0$, $2s^0$, and $2p^0$ are Hartree-Fock wave functions which were taken from Clementi.[23] For the bound states, Eqs. (12), (14), and (15) represent eigenvalue equations with discrete ϵ_{nl} while for the continuum states, $\epsilon_{kl} = \frac{1}{2} k^2$. The radial Eqs. (12) and (14) are obtained by the usual functional minimization of the energy of the atom with respect to variations in the radial functions $P(ns; r)$ and $P(np; r)$. The Eq. (15) for nd states requires a little explanation especially in respect to the numerical coefficients of the Y_k terms in exchange. There is a certain amount of arbitrariness[3] in the selection of these terms. The choice we used was to take the average of the one-electron potentials for the three configurations $(2p_{+1}{}^+ 2p_{-1}{}^+ n d_0{}^+)$, $(2p_{+1}{}^+ 2p_0{}^+ nd_{-1}{}^+)$, and $(2p_0{}^+ 2p_{-1}{}^+ nd_{+1}{}^+)$ which conserve the total $M_L = 0$ and $M_S = \frac{3}{2}$ for the atom.[24]

The matrix elements of the one-electron potential V^{N-1} between two one-electron states i_l and k_l can be written down using the forms of the radial equations (12), (14), and (15). For calculations by diagrammatic techniques, one has to represent these matrix elements in terms of diagrams.[2-4] For instance, the matrix elements of V^{N-1} between two s states or two p states can be represented as shown in Fig. 3. In comparing the diagrams in Figs. 3a and 3b with the radial equations (12) and (14), we have to remember that the hole and particle wave functions in the diagrams involve both radial and angular components as in Eq. (11). The last diagram in Fig. 3b uses a vertex ---- $\otimes$ which is a compact notation for the combination of Y_2 terms of Coulomb and exchange type in Eq. (14) with accompanying coefficients.

Since the one-electron potential we use corresponds to the restricted Hartree-Fock approximation, the basis functions obtained from Eqs. (12), (14), and (15) are the same for both spin states. The $2s$ and $2p$ basis functions obtained from Eqs. (12) and (14) are identical with the actual RHF functions ($2s^0$ and $2p^0$) for the atom. The $1s$ basis function, however, differs[2] slightly from the RHF $1s^0$ function, the latter being the solution of a somewhat different equation than (12). The difference in the one-electron energies ϵ_{1s} and $\epsilon_{1s}{}^0$ is more marked than the differences between the corresponding wave functions P_{1s} and $P_{1s}{}^0$. These differences will be carefully accounted for in the calculation of hfs diagrams, where the effects of the energy difference will come into play significantly through the ladder diagrams.

On substituting the diagrams from Fig. 3a for the potential vertex in Fig. 1a, there is considerable cancellation with other diagrams of Fig. 1, and the s-wave part of the first-order wave function is given by Fig. 4. The difference between P_{1s} and $P_{1s}{}^0$ shows up in diagrams of the type Figs. 4a, b, and c, which would cancel if there was no difference between these wave functions.
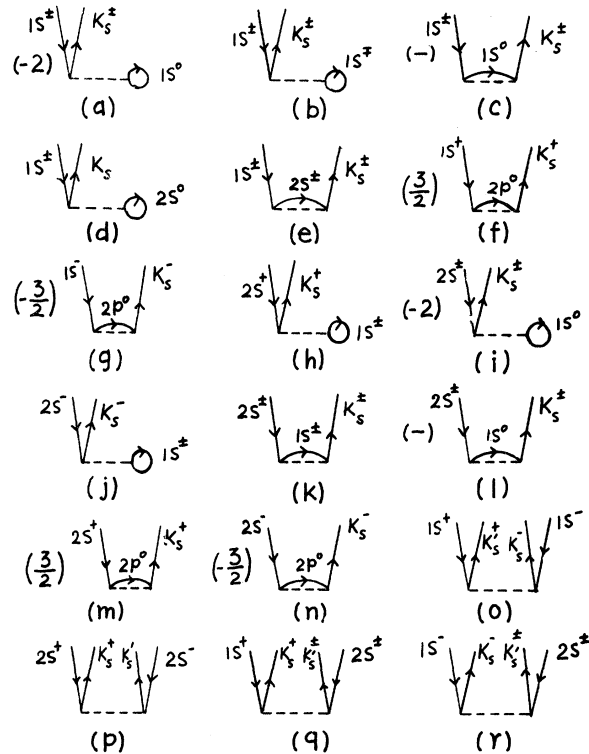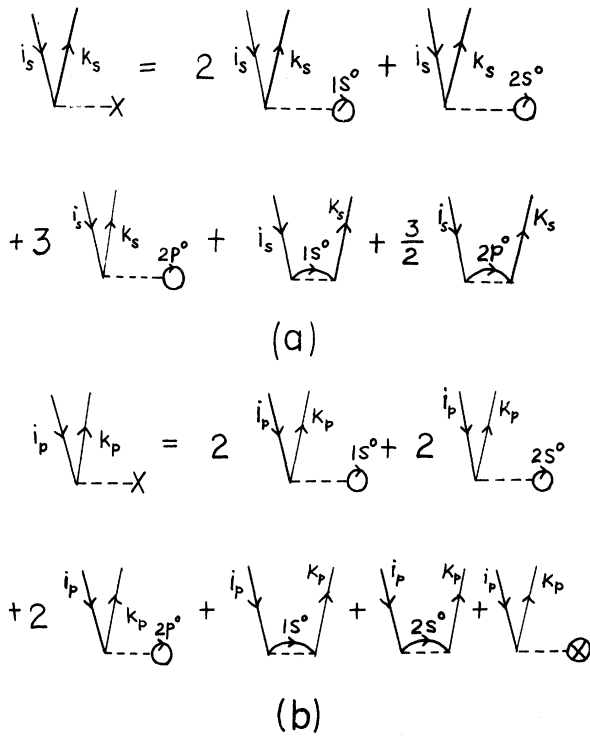
FIG. 3. Diagrammatic representation of the single-particle potential V. (a) Potential for $l = 0$ states. (b) Potential for $l = 1$ states.

FIG. 4. s-wave part of the first-order wave function.

B. Expectation Value of the hfs Operator

We can utilize either of two alternate approaches to hfs calculations. One way is to view the hfs interaction as an additional small perturbation $\mathcal{H}_{hfs}'$ on the atomic Hamiltonian (1)

$$\mathcal{H}_{hfs}' = \frac{16\pi}{3}\beta\mu_N \sum_{i=1}^{N}\delta(\vec{r}_i)\vec{s}_i \cdot \vec{I} - 2\beta\mu_N \left(\sum_{i=1}^{N}\frac{\vec{I}\cdot\vec{s}_i}{r_i^3} - \sum_{i=1}^{N}\frac{3(\vec{I}\cdot\vec{r}_i)(\vec{s}_i\cdot\vec{r}_i)}{r_i^5} \right), \tag{16}$$

where β is the Bohr magneton, μ_N the nuclear moment, and $\vec{I}$ and $\vec{s}$ are the nuclear and electron-spin operators. This additional perturbation, $\mathcal{H}_{hfs}'$ can be added to $\mathcal{H}'$ in (4) and the sum substituted in Eq. (8) to produce additional perturbation of the wave function. Use of this total wave function in Eq. (9) yields the linked-cluster expression for the total energy of the atom in the presence of $\mathcal{H}_{hfs}'$. However, since the hyperfine constant involves energy terms linear in μ_N, one has to retain only those terms in the perturbation expansion of (9) which contain a single order in the hfs perturbation. This procedure can be termed the energy expansion approach. An alternate procedure, is to calculate the expectation value of $\mathcal{H}_{hfs}'$ over the true ground-state wave function (8) and relate this to the hyperfine constant. This expectation-value vertex will be represented by $\sim\!\!\sim$ in hfs diagrams in conformity with earlier convention.[4] Both approaches of course lead to identical results and it is only as a matter of choice that we adopt the second procedure.

Since the ground state $(^4S_{3/2})$ of nitrogen atom is spherically symmetric, (zero total orbital angular momentum) the dipole-dipole term in (16) gives zero contribution and the hfs constant a is given by

$$a = \tfrac{16}{3}\pi(\beta\mu_N/IS)\langle \Psi_0 | \sum_{i=1}^{N}\delta(\vec{r}_i)s_{zi} |\Psi_0\rangle / \langle \Psi_0 |\Psi_0\rangle, \tag{17}$$

where $S = \tfrac{3}{2}$ is the total spin of the nitrogen atom. Introducing the notation

$$f = \sum_i \delta(\vec{r}_i)s_{zi} \tag{18}$$

for the spin-density operator, and expanding Ψ_0 in various orders, Eq. (17) may be re-expressed as

$$a = \frac{16}{3}\pi\frac{\beta\mu_N}{IS}\frac{\langle 0|f|0\rangle + \langle 0|f|1\rangle + \langle 1|f|0\rangle + \langle 1|f|1\rangle + \langle 0|f|2\rangle + \langle 2|f|0\rangle + \cdots + \langle m|f|n\rangle + \cdots}{\langle 0|0\rangle + \langle 1|1\rangle + \cdots + \langle m|n\rangle + \ldots} \tag{19}$$

where $\langle m|f|n\rangle = \langle n|f|m\rangle$ will be referred to simply as (m,n) diagrams.

C. Calculation of Basis Set and Normalization

The bound-state energies and wave functions were obtained by solving the radial equations (12), (14), and (15) using a program developed by Froese-Fischer.[25] This program utilized $\ln r$ as the independent variable which is particularly suitable for hyperfine properties since it effectively expands the region near the nucleus.

The continuum wave functions were obtained by solving the requisite differential equations and were normalized by fitting to the asymptotic solution

$$P(k,l;r) = (2/R)^{1/2}\sin[kr + \delta_l + \ln(2kr)/k - \tfrac{1}{2}l\pi] \tag{20}$$

at large values of $r = R$. This normalization procedure was carried out conveniently using a procedure based on WKB method.[26] In carrying out summations over excited states, the relation[2]

$$\sum_k = (2/\pi)\int_0^\infty dk \tag{21}$$

was employed. The integration over k was carried out using Gauss-Laguerre[27] quadrature procedure using 15 points, which was sufficiently accurate for our purpose. This procedure is particularly economical where double and triple integrations in k space are required in summing over intermediate states. For the radial space integration involved in matrix element calculations, we have used 1161 points in two meshes of appropriate size over the range $r = 0$ to $50\,a_0$.

IV. DIAGRAMS AND RESULTS

In this section we present the results of our calculation. We have included all hfs diagrams with up to two interacting vertices of $\mathcal{H}'$. That is, all $(0,1)$, $(1,0)$, $(1,1)$, $(0,2)$, and $(2,0)$ type diagrams have been considered. The $(0,0)$ diagrams give zero contribution to the hfs constant a, Eq. (19), since the unpaired p valence electrons have zero density at the nucleus and the spin-up and spin-down s electrons give equal and opposite contributions in the RHF approximation. The hfs in nitrogen atom owes its origin to the unsymmetric interaction between the three valence $2p^+$ electrons with the spin-up and spin-down core s electrons. This unsymmetric interaction is constituted partly of the exchange core-polarization effect[4,8−11] and partly the correlation with the core electrons and associated effects. In addition, the unsymmetric phase space available for the excited states, since the $2p^-$ states are empty, leads to further contributions to the hfs constant. The consequences of these observations in diagrammatic language manifest themselves in that the diagrams

contributing to hfs have at least one $2p^+$ hole line or one $2p^-$ particle line. The latter type of diagrams are called residue diagrams and their magnitudes are usually relatively small.

It is interesting to note that correlation among the $2p^+$ electrons cannot contribute to the hfs. The reason for this is that the excited configurations $(2p^+ns^+ms^+)$, which could make such contribution, have nonzero total angular momentum and therefore cannot mix with the $2p^3(^4S_{3/2})$ state. It can be shown (see the Appendix) that this ineffectiveness of the intrashell correlation among valence electrons in contributing to the hfs follows from a natural cancellation of diagrams and, in fact, this is true for all open-shell atoms.

(0,1) Diagrams

Because of the one-particle nature of the hfs operator, the only (0, 1) contribution comes from the "exchange core-polarization" diagrams in Fig. 5. The negative sign in front of the spin-down part of the exchange-polarized core wave function is multiplied by a -1 factor from the s_z part of the hfs operator, so that the net effect is to add the spin-up and spin-down contributions. The algebraic expression for this (0,1) diagram, pertaining to the first-order contribution from s core electrons to hfs is given by

$$\sum_{k_s} \frac{\langle i|f|k_s\rangle \langle k_s 2p|1/r_{12}|2p i\rangle}{\epsilon_i - \epsilon_{ks}}, \quad i = 1s \text{ or } 2s,$$

where the summation over k_s includes both bound particle states and integration over the continuum states. The difference of spin-up and spin-down core wave functions comes from their unsymmetric exchange interaction with the valence $2p^+$ electrons. This (0,1) diagram, or its modified
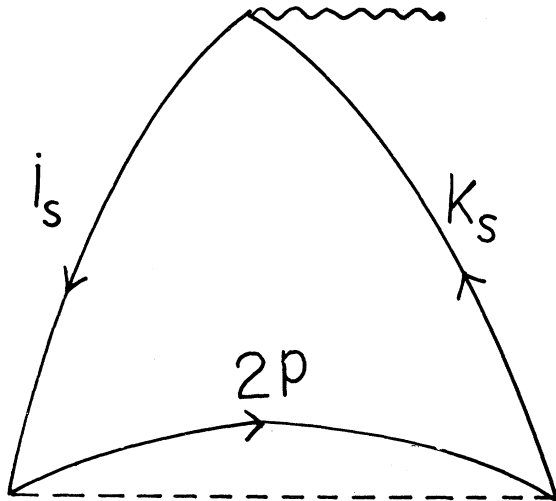
form to be discussed next, is comparable in principle to the perturbation energy one evaluates in the EP or MP methods.[16,17]

In the derivation of the linked-cluster result of the BG theory, there will arise certain exclusion principle violating (EPV) diagrams which represent important physical effects.[2-4] The first class of EPV diagrams are the hole-hole (h-h) type which arises from the factorization of the unlinked clusters. With our definition of V^{N-1}, the h-h type EPV diagrams will occur for $1s$ hole states but not for $2s$ hole states. The EPV h-h diagrams are illustrated in Figs. 6a and 6b. Physically, these EPV diagrams occur because in our calculation the $1s$ state is generated by a potential that has, besides interactions with $2p$ electrons, direct interactions with two $1s^0$ electrons, one $2s(2s^0)$ electron, and exchange interaction with one $1s^0$. The actual $1s$ electron, however, while interacting similarly with the $2p$ electrons, should see direct interactions with one $1s$ and two $2s$, and one exchange with $2s$ electron. The h-h diagrams (6a) and (6b) correct for the difference between these potentials. The effect of the slight difference between $1s$ and $1s^0$ wave functions will be omitted in this calculation.

Figures (6c) and (6d) refer to the hole-particle (h-p) ladder diagrams. Each of the diagrams (6c) and (6d) represents in a compact form two distinct series of diagrams, namely, one with $1s$ exchange or coulomb ladders, and the other in-

(a)

(b)

(c)

(d)
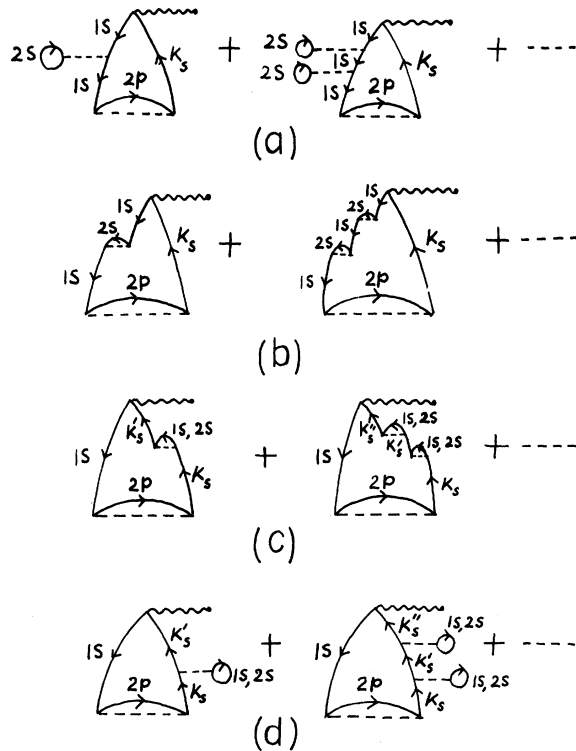
FIG. 6. Hole-hole and hole-particle ladder corrections to Fig. 5. Correction to $1s$ potential is represented by (a) and (b), whereas (e) and (d) represent corrections to excited state potential.

FIG. 5. Exchange core-polarization diagram, referred to as (0, 1) diagram in the text. i denotes hole states and k_s denote excited s states. The wiggly line at the top vertex represents hyperfine contact operator.

volving $2s$ ladders. These diagrams arise from an incomplete cancellation between the single-particle vertices associated with V^{N-1} potential and passive unexcited states. Physically, the origin of Diagrams (6c) and (6d) can be explained by the fact that when the k_S state is excited from the $1s$ state, it should "see" one $1s$ and two $2s$ orbital electrons, which is not the way k_S was generated from our choice of V^{N-1} potential. Some of these diagrams, for example the (6c) diagram with $1s$ ladder attached to the $1s$ hole diagram, can be loosely referred to as EPV diagrams although its origin is different.

These h-h and h-p ladder corrections can be summed to all orders as a geometric series, resulting in a shifted energy denominator[2,3] of the (0,1) diagram. One then gets the following correction factors to the $1s$ state core-polarization diagrams (Fig. 5):

(h-h) EPV   (6a) + (6b) = $\dfrac{\epsilon_{1s} - \epsilon_{ks}}{\epsilon_{1s} + \delta\epsilon_{1s} - \epsilon_{ks}}$,   (22)

where

$\delta\epsilon_{1s} = \langle 1s2s \mid \dfrac{1}{r_{12}} \mid 1s2s \rangle - \langle 1s2s \mid \dfrac{1}{r_{12}} \mid 2s1s \rangle$;

(h-p)   (6c) + (6d) = $\dfrac{\epsilon_{1s} - \epsilon_{ks}}{\epsilon_{1s} - \epsilon_{ks} - \delta\epsilon_{ks}}$,

where

$\delta\epsilon_{ks} = - \langle k_s 1s \mid \dfrac{1}{r_{12}} \mid k_s 1s \rangle + \langle k_s 2s \mid \dfrac{1}{r_{12}} \mid k_s 2s \rangle$

$+ \langle k_s 1s \mid \dfrac{1}{r_{12}} \mid 1sk_s \rangle - \langle k_s 2s \mid \dfrac{1}{r_{12}} \mid 2sk_s \rangle$.

                       (23)

The h-h correction factor comes out as 4% while the h-p correction is 1.38%. The results for the exchange core-polarization diagrams (with and without ladder for the $1s$ state) are tabulated in Table I. The major contribution to both the $1s$ and $2s$ diagrams (92 and 97%, respectively) arose from the continuum excited states. Similar relative contributions from bound and continuum ex-

cited states were also found for the higher-order diagrams, (1,1) and (0,2). In this respect the situation is similar to the lithium-atom ground-state result.

(1,1) Diagrams

A first inspection of the (1,1) diagrams indicates that their number is rather large. However, after carrying out systematic cancellations along the lines indicated in Sec. III, the surviving hfs diagrams are not too many and are shown in Fig. 7. The corresponding numerical results from these diagrams are given in Table II. Diagram (7a) comes from the correlation interaction of $2p^+$ electron with the s-core states, (7b) being the exchange analog of (7a). Diagram (7c) is the
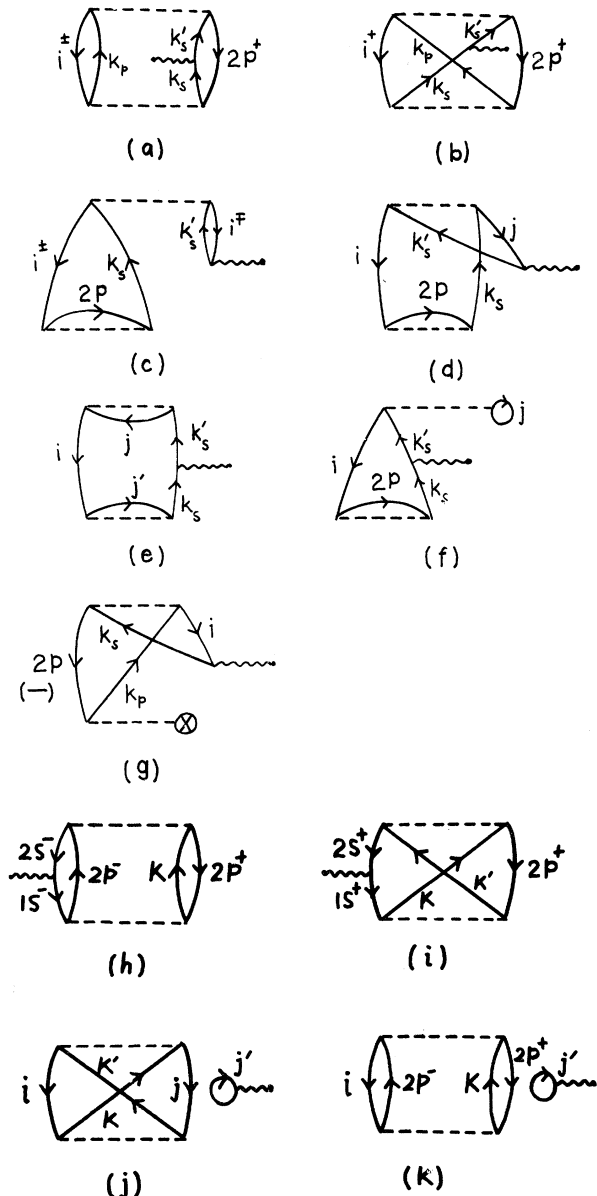
FIG. 7. (1, 1) hfs diagrams.

TABLE I. Core-polarization contributions of Fig. 5.

Hole state	Contribution (Mc/sec)[a]
$i = 1s$	$-47.823\,85$
	$-49.740\,10$[b]
	$-50.429\,55$[c]
$i = 2s$	$+56.220\,19$
Total	$+5.790\,64$

[a]Contributions from the bound states $n > 8$ were estimated by the n^{-3} rule and amounted to less than 0.02%. [See Ref. 2 and H. A. Bethe and E. E. Salpeter, Quantum Mechanics of One- and Two-Electron Systems (Academic Press Inc., New York, 1957) p. 18.]

[b]After including hole-hole ladder corrections according to Figs. 6(a) and (b).

[c]After inclusion of hole-hole and hole-particle ladders, the latter being shown in Figs. 6(c) and (d).

TABLE II. Contributions from (1, 1) diagrams.

Diagram	Participating hole states	Contribution (Mc/sec)
(7a)	$i = 1s^{\pm}$	0.286 95
	$i = 2s^{\pm}$	1.413 51
(7b)	$i = 1s^{+}$	0.170 97
	$i = 2s^{+}$	1.799 34
(7c)	$i = 1s$	−0.984 79
	$i = 2s$	2.802 24
(7d)	$i = 1s, \quad j = 2s$	−0.058 59
	$i = 2s, \quad j = 1s$	0.131 60
(7e)	$i = 1s, \quad j = 2p, \quad j' = 2s$	−0.111 69
(7f)	$i = 1s, \quad j = 2s$	0.077 76
(7g)	$i = 1s^{+}$	0.132 51
	$i = 2s^{+}$	−0.382 65
(7h)		0.091 03
(7i)		−0.227 20
(7j)	$i = 2p, \quad j = 1s_{+}^{+}, \quad j' = 1s^{-}$	0.191 34
	$i = 2p, \quad j = 2s^{+}, \quad j' = 2s^{-}$	−0.314 23
(7k)	$i = 1s^{-}, \quad j' = 1s^{+}$	0.144 91
	$i = 2s^{-}, \quad j' = 2s^{+}$	0.089 67
Total		5.252 69

result of a combination of intrashell correlation and exchange core-polarization. The "exchange"-type diagram in (7d) represents a cross interaction between the intershell correlation between the $1s$ and $2s$ electrons and exchange-polarized cores. The barrel-shaped diagram (7e) is the net second-order term arising from the exchange-polarized wave function. Diagram (7f) arises from a combination of the exchange-polarized $1s$ core (Fig. 4) and the "correction" term (Fig. 4) for the $1s$ core. Diagram (7g) comes from the interaction of $2p^{+} - 1s^{+}$ correlation and the extra potential term (Fig. 3) mentioned in Sec. III.

Diagrams (7h) through (7k) are somewhat distinct from the rest in that the hfs vertex is attached to hole lines. Diagrams (7h) and (7i) are similar to Diagrams (7a) and (7b), where the hfs vertex is attached to particle lines. The unlinked diagrams (7j) and (7k) arise naturally from the $\langle 1 \, | f | \, 1 \rangle$ term in Eq. (8) using the linked-cluster expansion for the wave function $|1\rangle$. If one had made binomial expansion of the normalization factor in the denominator in Eq. (19) it could provide the corresponding unlinked terms of the opposite sign. The net result then agrees with the linked-cluster energy expansion method.

(0,2) Diagrams

There is a greater similarity between (0, 2) and (0, 1) diagrams with respect to spin cancellations than was the case for (1, 1). This is because for both (0, 1) and (0, 2) diagrams, the hfs vertex involves one-hole line and one-particle line. The greater cancellation relative to (1, 1) diagrams is a great advantage because the (0, 2) diagrams are

much more numerous before cancellation. The systematic reduction gives the net diagrams in Fig. 8, their respective values being given in Table III. Diagram (8a) represents a residue diagram associated with the instantaneous polarization of s electrons with other electrons (both s and p). Since the s electrons in nitrogen atom are in completely filled core states, the net contribution from this polarization effect would cancel over the two spin states except for the unsymmetric phase space available to particle p states. Thus the net effect in (8a) represents the fact that s^{-} electrons can be excited into $2p^{-}$ state while s^{+} electrons cannot. Diagram (8b) is similar in nature to (8a) except that the second $\mathfrak{K}'$ vertex is now attached to a hole line on the left instead of a particle line. However, only a part of this diagram is residue like in nature, namely the one involving $1s^{-}$ or $2s^{-}$ hole states on the right. Diagrams (8c) and (8d) are exchange counterparts of (8a) and (8b), the exchange being allowed only for spin-up electrons. Diagrams (8e) and (8f) represent an interplay between exchange core-polarization and correlation and consistency effects. Diagrams (8h) really represent two distinct types of physical effects. For $(i = 1s, \; j = 2s)$, the diagram describes an indirect exchange core-polarization process. Thus the exchange interaction with $2p$ electrons makes

(a)   (b)

(c)   (d)

(e)   (f)

(g)   (h)
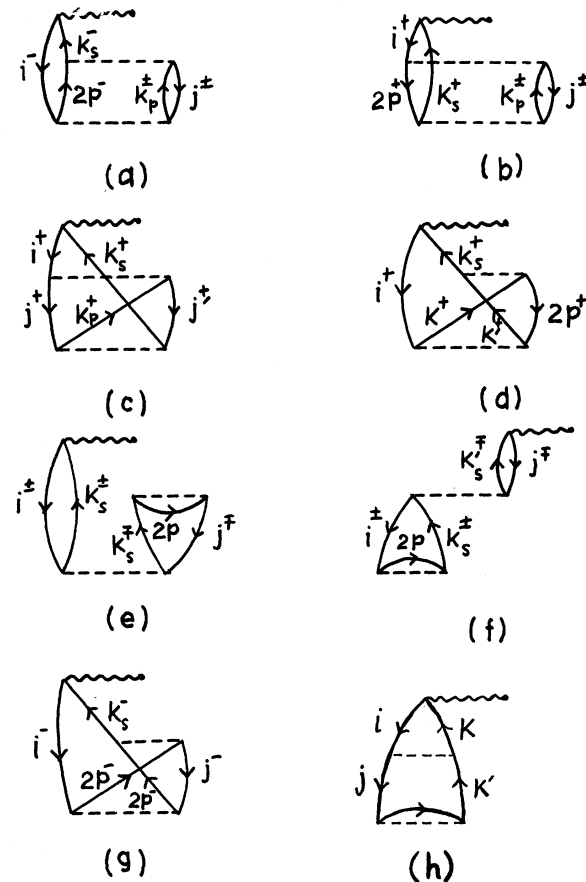
FIG. 8. (0, 2) hfs diagrams.

TABLE III. Contribution from $(0, 2)$ diagrams.

Diagram	Participating hole states	Contribution (Mc/sec)
(8a)	$i = 1s^-$, $j = 1s^+$	0.430 90
	$i = 1s^-$, $j = 2s^\pm$	$-0.003\,76$
	$i = 1s^-$, $j = 2p^+$	0.887 122
	$i = 2s^-$, $j = 1s^\pm$	$-0.910\,15$
	$i = 2s^-$, $j = 2s^+$	$-0.522\,61$
	$i = 2s^-$, $j = 2p^+$	$-1.645\,34$
(8b)	$i = 2s^+$, $j = 2s^-$	$-0.600\,66$
	$i = 2s^+$, $j = 1s^\pm$	$-0.771\,18$
	$i = 1s^+$, $j = 1s^-$	0.485 54
	$i = 1s^+$, $j = 2s^\pm$	$-0.080\,40$
(8c)	$i = 1s^+$, $j = 2s^+$, $j' = 2p^+$	$-0.348\,30$
	$i = 1s^+$, $j = 2p^+$, $j' = 2s^+$	$-0.785\,83$
	$i = 2s^+$, $j = 2p^+$, $j' = 1s^+$	$-0.295\,03$
	$i = 2s^+$, $j = 1s^+$, $j' = 2p^+$	$-0.200\,10$
(8d)	$i = 1s^+$	$-0.803\,58$
	$i = 2s^+$	$-0.395\,96$
(8e)	$i = 1s^\pm$, $j = 1s^\mp$	$-0.610\,142$
	$i = 2s^\pm$, $j = 2s^\mp$	1.973 35
(8f)	$i = 1s^\pm$, $j = 1s^\mp$	$-1.591\,35$
	$i = 2s^\pm$, $j = 2s^\mp$	4.775 59
(8g)	$i = 1s^-$, $j = 2s^-$	$-0.003\,75$
	$i = 2s^-$, $j = 1s^-$	0.013 46
(8h)	$i = 1s$, $j = 2s$	1.080 70
	$i = 2s$, $j = 1s$	$-0.600\,70$
	$i = 1s$, $j = 2p$	2.403 15
	$i = 2s$, $j = 2p$	$-2.812\,22$
Total		$-0.931\,31$

FIG. 9. $(0, 2)$ EPV diagrams. The notation $\equiv$ indicates the equivalence of the two alternate diagrams.

the wave function of $2s^\pm$ states different, which in turn produce a core polarization of the $1s^\pm$ states. A similar interpretation applies for $(i = 2s, \, j = 1s)$. The two diagrams (8h) with $(i = 1s$ or $2s, \, j = 2p)$ are somewhat closer in physical meaning to Diagrams (8f). They describe how the core-polarization diagrams in Fig. 5 are influenced by the consistency effects arising from exchange between the $2p$ electrons.

In addition to these $(0, 2)$ diagrams, one also has the diagrams in Fig. 9, which are EPV diagrams [analogous to the second class of EPV diagrams for the $(0, 1)$ case] associated with the incomplete cancellation of V^{N-1} vertex and passive unexcited vertices. The results of these EPV diagrams are listed in Table IV.

It is appropriate to remember here that the values of diagrams of (m, n) type, with $m \neq n$, have to be multiplied by a factor of two to take account of the equal contribution from the (n, m) type, otherwise referred to as time-reversal symmetry. This factor of two has been included in the results tabulated for all of the $(0, 1)$ and $(0, 2)$ diagrams and for some of the $(1, 1)$ diagrams wherever necessary. Secondly, in the entries for various $(1, 1)$ and $(0, 2)$ diagrams in Tables II, III, and IV, we have included h-h ladder corrections following the procedure outlined for $(0, 1)$ diagrams. The effect of h-p ladders has not been included

since their calculation is an order-of-magnitude more difficult. However, it was already seen in the $(0, 1)$ that the (h-p) ladder corrections was only a third as important as h-h ladders. Since the values of the individual unmodified $(1, 1)$ and $(0, 2)$ diagrams are an order-of-magnitude smaller than in the $(0, 1)$ case, the effect of neglect of h-p ladder corrections for the former diagrams is not expected to be very important.

The total contributions from the $(0, 1)$, $(1, 1)$, and $(0, 2)$ diagrams and their sum are listed in Table V and compared with experiment. The entries in

TABLE IV. Contributions from $(0, 2)$ EPV diagrams.

Diagram	Participating hole states	Contribution (Mc/sec)
(9a)	$i = 1s^+$	$-2.722\,27$
	$i = 2s^+$	$-0.017\,82$
(9b)	$i = 1s^+$	0.459 73
	$i = 2s^+$	2.923 43
(9c)	$i = 1s^+$, $j = 1s^+$	0.485 54
	$i = 2s^+$, $j = 2s^+$	$-0.600\,66$
Total		0.527 95

TABLE V. Net contributions from (0, 1), (1, 1) and (0, 2) diagrams.

| | Contribution (Mc/sec) | |
Class of diagram	unnormalized	normalized
(0, 1)	5.790 643	5.708 10
(1, 1)	5.252 69	5.177 82
(0, 2)	− 0.403 36	− 0.397 60
Total		10.488 32
Experiment		10.45 ± 0.000 07

Table V for the (0, 1), (1, 1), and (0, 2) diagrams are a little different from the corresponding sums listed in Tables I–IV. The reason is that the numbers in Table V are normalized by including the normalization factor in the denominator of Eq. (19). Up to second order, only the (1, 1) normalization diagrams in Fig. 10 survive. The sum of the contributions from these diagrams lead to a normalization constant of 1.014 46 for the denominator in Eq. (19).

V. DISCUSSION

In this section, we shall first try to draw some inferences from the individual contributions in Tables I–V concerning the importance of various physical effects that can contribute to the hfs. Subsequently, we shall carry out a comparison between our results for the hfs constant and earlier theoretical values[8,12,18,19,21] as well as experiment.

The largest effect, as expected, comes from exchange core-polarization (ECP), the (0,1) diagrams. However, from Table I, the 1s and 2s cores are seen to give contributions that are nearly equal but opposite in sign. The net contribution is therefore only about 10% of those from the individual states. This trend of opposite sign for the hfs from 1s and 2s orbitals seems to persist in our higher-order calculations. The (0, 1) results, as mentioned before, should be equivalent to those by the EP and MP methods.[16,17] However, in carrying out calculations with the EP or MP methods, one often employs a localized approximation[17] for the potential. Such an approximation tends to overestimate the exchange effect and could lead to slightly larger ECP results.[4,6] This point is borne out in the present case by a comparison of results in Table I with MP contributions[28] from 1s and 2s states of − 50.8 and 60.7, respectively. While the individual state results by both procedures agree reasonably well with each other, the net hfs constant, being the dif-

ference of nearly equal numbers, shows a much greater variation (nearly a factor of 2) from one procedure to the other.

An inspection of the (1, 1) diagrams in Fig. 7 and their values in Table II reveals that there are broadly two classes of diagrams that make important contributions to hfs. The first class of diagrams is symbolized in (7a) and (7b) in which the hyperfine vertex is attached to a particle s line arising out of correlation effects in which the p-hole states take part. Physically, these diagrams represent the effects of acquisition of s character by the unpaired p electrons as a result of their correlation interaction with s-hole states. Since these electrons are in spin-up states, we expect a positive contribution to hfs from this process. This fact is borne out by the results listed in Table II. In addition, one notices that the diagrams in which 2p correlates with 2s dominate over those in which 1s is involved. This is to be expected since the 2p density overlaps the 2s density more strongly than it does to the 1s.

The second major class of (1, 1) diagrams, represented by (7c) and (7d), are characterized by an intermixing between correlation and ECP effects. In these diagrams, the hfs vertex is attached to a segment that involves a hole s state. As is the case of the (0, 1) ECP diagrams, the 1s contribution is negative and opposite in sign to that for 2s. The diagrams involving 2s are again larger in magnitude than those associated with 1s, the ratio being, however, smaller than the case of (7a) and (7b).

In addition to these two major classes of (1, 1) diagrams, we also have the two other classes which encompass (7e) through (7k). Of these, (7e), (7f), and (7g) owe their origin to our specific choice of V^{N-1} potential. Diagrams (7e) and (7f) represent an interplay between ECP effects and interaction with passive, unexcited states, and are numerically much less significant than diagrams considered previously. The diagram (7g) is the only survivor of a set of diagrams that result from a combination of correlation and the special $---- \otimes$ vertex in Fig. 3, after spin and potential cancellation has been made. Its contribution, while more important than (7e) or (7f), is much smaller than the leading diagrams of the (1, 1) set. The diagrams (7h) through (7k) are found to be individually small but significant. However, owing to mutual cancellation among themselves, the net contribution is seen to be rather small.

Among the (0, 2) diagrams, (8a) and (8b) can be characterized physically as representing the mutual polarization of 1s and 2s states by each other. These diagrams are, however, only residue diagrams and would vanish, were it not for the unequal p-particle phase space available to up and down spin states. Diagrams (8c) and (8d) are exchange counterparts of (8a) and (8b). From Table III, we find that these diagrams are individually comparable to leading (1, 1) diagrams. Diagram (8e) represents an interplay between ECP and correlation effects while the diagram (8f) represents similar interaction between ECP and consistency effects. Physically these two

(a)   (b)   (c)
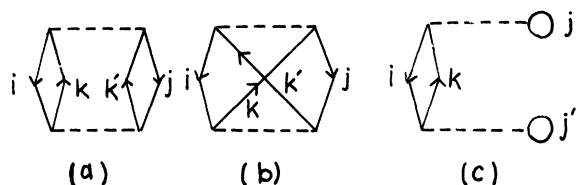
FIG. 10. Normalization diagrams.

diagrams may be described as follows. One of the s states of a core shell get exchange polarized and then interacts with other core electrons in the same shell via correlation or consistency-type effects. Like (7c) and (7d), the diagrams (8e) and (8f) involve a core-polarization limb and would be expected to have opposite contributions from 1s and 2s hole states as indeed found in Table III. Another interesting result is that the diagrams (8e) and (8f) combine and give a substantial positive contribution, which nearly neutralizes the total sum of (8a) through (8d) which is negative. This accounts for the small net contribution of (0,2) diagrams in Table V. It is worthwhile to remark here that the diagrams (7c) and (8e) may be shown by algebraic manipulation to add up to (8f). From Tables II and III, the numerical values of these diagrams obtained separately do, in fact, satisfy this equality, thus acting as a check on our numerical procedure.

Finally, the net (0,2) EPV diagrams (9a), (9b), and (9c), originating from incomplete cancellation effects associated with the V^{N-1} potential, are also seen from Table IV to be of substantial size individually but add up to a small contribution which does not substantially alter the total (0,2) result. It is interesting that in contrast to some other diagrams where 1s and 2s hole states were involved, in the diagram (9a) the 1s contribution is much larger than 2s.

We shall next turn to a comparison between our results for the hfs constant with those of earlier workers and experiments which are listed in Table VI. Our final result is in excellent agreement with experiment and is taken from Table V with an estimate of probable error added. This error estimate is arrived at from a consideration of various sources that could be important. The first source is the neglect of nonladder higher-order diagrams beyond (0,2). We have examined two typical higher-order diagrams shown in Figs. 11; (11a) being a (0,3) diagram and (11b) a (1,2). Including both 1s and 2s state contributions,
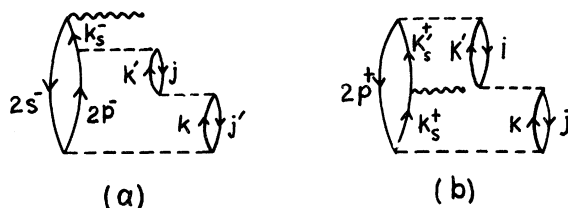
FIG. 11. Some third-order diagrams.

the diagram (11a) gives 0.002 172 Mc/sec. This diagram may be compared with the lower-order diagram of this family as characterized by Fig. (8a), whose total contribution from Table III is seen to be − 1.763 84 Mc/sec. This is three orders of magnitude larger than (11a). Similarly the (1,2) diagram in (11b) can be compared with the (1,1) diagram in (7a). From (11b), including 1s and 2s contributions, we get 0.002 11 Mc/sec which is again three orders of magnitude smaller than the result for the (1,1) Diagram (7a) in Table II. We do not anticipate that any other higher-order diagrams will be of larger order of magnitude than the two typical ones (11a) and (11b) that we have calculated. Further, although the number of higher-order diagrams is more numerous than lower-order ones, we also expect more cancellations of the type that occurred for (0,2). From these considerations, we feel that a conservative estimate of the error in the hfs constant due to higher-order diagrams is ±0.05 Mc/sec. A second source of error is our neglect of (h-p) and (p-p) ladders beyond the (0,1) diagram. For the (0,1) diagram, the (h-p) ladder changed the result by about 1.3% which was substantial in effect in that case since the individual (0,1) diagrams were large. On the other hand, the (1,1) and (0,2) diagrams all have contributions an order of magnitude or more smaller than (0,1), thus the neglect of the (p-p) and (h-p) ladders is not expected to be as serious.

TABLE VI. Comparison of present results with earlier work and experiment.

Method		1s contribution Mc/sec	Result 2s contribution Mc/sec	Total Mc/sec	Ref.
UHF (numerical)		−79.8	100	20.2	8
(analytic)		−75	108	33	a
MP		−50.8	60.7	9.9	28
Cross-variational		−36.4	43.7	7.3	19
CI (perturb-	six basis	−46	54	8	12
ation approach)	seven basis	−49	54	5	12
CI	six basis	−45	58	13	12
	seven basis	−47	58	11	12
Bethe−Goldstone				10.87	18
Present calculation				10.49± 0.15	
Experiment				10.45 ± 0.000 07	b

[a] R. K. Nesbet and R. E. Watson quoted in Ref. 12.
[b] Anderson, Pipkin, and Baird. Ref. 20.

A conservative estimate of the error due to this source is about 1% of the total contribution from all the (1,1) and (0,2) diagrams, that is, ±0.05 Mc/sec. Among other possible sources of error are the neglect of relativistic effects, which are not expected to be very important for a light atom like nitrogen. A conservative estimate may again be arrived at by comparing with lithium and sodium atoms, for which the relativistic corrections to hfs are 0.3 and 1%, respectively. Thus a ±0.5% error, equivalent to ± 0.05 Mc/sec. seems to be appropriate for relativistic effects.

The total estimated error in Table VI is arrived at from a combination of these three sources. It should be noted that in contrast to earlier calculations,[2-5] the use of limited k integration is no longer an important source of error because of our use of Gauss-Laguerre integration technique.

A general feature of all the earlier results listed in Table VI, is that $1s$ contributions are all negative, while $2s$ ones are all positive, in keeping with the results of (0,1) diagrams in BG theory. The first row in Table VI gives the UHF results obtained by Goodings[8] who solved the self-consistent UHF equations numerically. The UHF result is almost twice our total result and more specifically, the individual $1s$ and $2s$ UHF contributions are substantially larger than the ECP contributions we obtained in Table I. There is some reason for not expecting one-to-one correspondence between individual shell UHF results and ECP contributions by our perturbation technique. The UHF approximation incorporates self-consistency and an uncertain[11] amount of correlation. These effects are included in BG theory in the higher-order diagrams (1,1) and (0,2). It seems to us, however, that the major reason for discrepancy between the UHF results and our ECP results is that differences of rather large numbers from spin-up and spin-down states are involved in the UHF procedure, with consequent loss of accuracy. The second row in Table VI illustrates this point further. These are also UHF results but they are obtained analytically from a limited basis set. The difference between numerical and analytic UHF calculations emphasizes the care that must be used in analytic variational calculations.

The MP results in the third row are much better comparable with the BG (0,1) results and this comparison has already been remarked earlier. The cross-variational results in the fourth row are not very conclusive since they involve extremization of perturbation energy rather than minimization, thus requiring an extensive test of convergence which has not been carried out. Nevertheless it is interesting to note that in view of the perturbation character of this calculation, the individual state contributions are closer to the corresponding BG results than UHF.

Although the fifth and sixth rows of Table VI are termed CI (configuration interaction) results,[12] they really correspond to a perturbation formulation for a PUHF theory.[10,11] The difference between RHF and PUHF wave functions is obtained by a first-order admixture of singly excited configurations. Again, being a perturbation approach,

their results for individual shells are closer to our corresponding results in Table I. The substantial difference between the fifth- and sixth-row results in changing from a basis set of six functions to seven, again illustrates the caution one has to use in analytic expansion approaches. The seventh and eighth rows give the result of CI calculation in which some doubly excited configurations are included, in addition to singly excited ones of the perturbation approach. These CI results thus incorporate some correlation, but no definitive conclusions can be made from them in view of the observed substantial variation in going from a six basis set to a seven basis one.

Finally, the Bethe-Goldstone technique as formulated by Nesbet,[18] makes a neat separation into single, double, triple, and larger number of particle excitations in dealing with many-body effects. The results of this procedure including the effect of three-particle excitations is seen (Table VI) to be in good agreement with experiment and our results. The reamining discrepancy between Nesbet's results and experiment can perhaps be removed by the use of a more extended basis set in the Bethe-Goldstone procedure.

VI. CONCLUSION

The BG theory for nitrogen atom has been shown in this paper to yield excellent results as compared to experiment. Its success for a more complicated situation than in the earlier application to lithium atom[4,6] increases our confidence in its applicability. In contrast to the lithium situation, correlation and core-polarization results are here comparable in magnitude. The major contribution to correlation effects seems to arise from the admixture of s character in the unpaired spin orbitals by virtue of correlation with the s-shell electrons. Also the entire contribution to the hfs constant appears to arise from diagrams of first and second order alone. These observations lead us to expect that the application of BG theory to more complex atoms is well within the realm of possibility and would be very interesting to pursue.

APPENDIX

The possible p-p correlation diagrams that can contribute to hfs of nitrogen atom are shown in Figs. (12a-h). Each diagram includes, besides the requisite radial integrals, the angular factors corresponding to the upper and lower vertices, some of which are indicated below the diagrams for reference. Comparing, for example, Diagram (12a) with Diagram (12b), it is easily seen that these diagrams cancel each other, since the
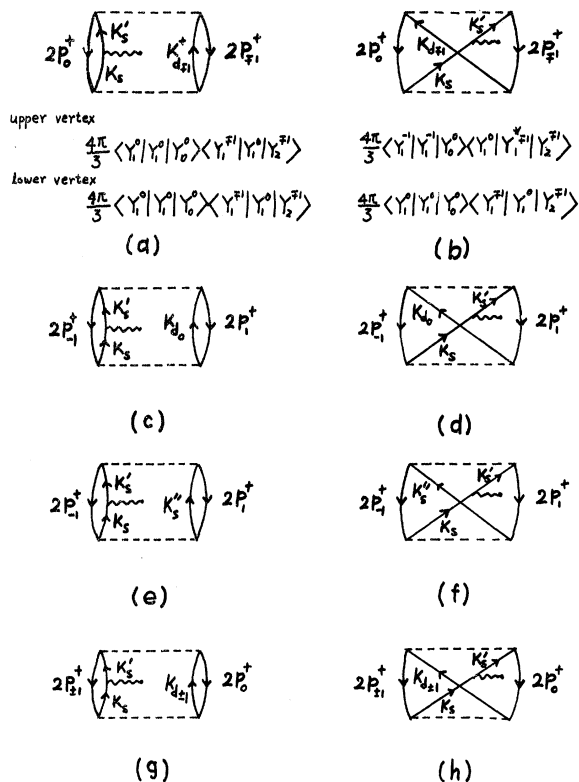
FIG. 12. Valence p−p correlation diagrams for hfs in nitrogen atom.
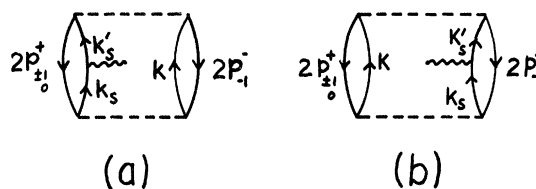
FIG. 13. Additional p−p correlation diagrams occuring in the oxygen atom. k denotes either excited s or d states.

angular factors and radial integrals of both diagrams are the same and the signs of the diagrams are opposite. In the same fashion, it may be shown that Diagrams (12c) and (12d), (12e) and (12f), (12g) and (12h) all cancel in pairs. These cancellations explain the vanishing contribution from p-p correlation effects to hfs.

A similar cancellation of correlation diagrams for valence p electron to hfs can be demonstrated in oxygen atom as well. For the oxygen atom, $(1s^2 2s^2 2p^4; {}^3P_1$ state) in addition to the diagrams in Fig. 12, one can have the diagrams in Figs. 13a and 13b. However, because of the opposite spins involved, the diagrams (13a) and (13b) cancel each other, leading again to a zero total contribution. The same cancellation of p-p diagrams can be easily demonstrated for other incomplete p-shell atoms.

*Supported by the National Science Foundation. Portions of this work were reported briefly at the American Physical Society meeting at Washington, D. C., April 22–25, 1968.

[1]J. Goldstone, Proc. Roy. Soc. (London) A239, 267 (1957).

[2]H. P. Kelly, Perturbation Theory and its Application in Quantum Mechanics, edited by C. H. Wilcox (John Wiley & Sons, Inc., N. Y., 1966), p. 215; Phys. Rev. 131, 684 (1963); 136, B896 (1964).

[3]H. P. Kelly, Phys. Rev. 144, 39 (1966).

[4]E. S. Chang, Robert T. Pu, and T. P. Das, Phys. Rev. 174, 1 (1968).

[5]E. S. Chang, Robert T. Pu, and T. P. Das, Phys. Rev. 174, 16 (1968).

[6]J. D. Lyons, Robert T. Pu, T. P. Das, and E. S. Chang, Bull. Am. Phys. Soc. 12, 1116 (1967).

[7]C. Matsubara, N. C. Dutta, Robert T. Pu, and T. P. Das, Bull. Am. Phys. Soc. 13, 373 (1968).

[8]D. A. Goodings, Phys. Rev. 123, 1706 (1961).

[9]R. E. Watson and A. J. Freeman, Phys. Rev. 123, 2027 (1961).

[10]W. Marshall, Proc. Phys. Soc. (London) A78, 113 (1961).

[11]V. Heine, Czech. J. Phys. 13, B619 (1963).

[12]N. Bessis, H. Lefebvre-Brion, and C. M. Moser, Phys. Rev. 124, 1124 (1961).

[13]R. K. Nesbet, Proc. Roy. Soc. (London) A230, 312 (1955).

[14]N. Bessis, H. Lefebvre-Brion, C. M. Moser, A. J. Freeman, R. K. Nesbet, and R. E. Watson, Phys. Rev. 135, A588 (1964).

[15]P. Bagus and A. J. Freeman, Bull. Am. Phys. Soc. 13, 481 (1968).

[16]M. H. Cohen, D. A. Goodings, and V. Heine, Proc. Phys. Soc. (London) 73, 811 (1959).

[17]G. D. Gaspari, W. M. Shyu, and T. P. Das, Phys. Rev. 134, A852 (1964); 152, 271 (1966); L. Tterlikkis, S. D. Mahanti, and T. P. Das, Phys. Rev. 176, 10 (1968).

[18]R. K. Nesbet, La Structure Hyperfine des Atomes et des Molecules, edited by R. Lefebvre and C. Moser (Centre National de la Recherche Scientifique, Paris, 1967), p. 87.

[19]T. P. Das and A. Mukherjee, J. Chem. Phys. 33, 1808 (1960).

[20]M. A. Heald and R. Beringer, Phys. Rev. 96, 645 (1954); W. Holloway and R. Novick, Phys. Rev. Letters 1, 367 (1957); L. W. Anderson, F. M. Pipkin, and J. C. Baird, Phys. Rev. 116, 87 (1959).

[21]N. Bessis, H. Lefebvre-Brion, and C. M. Moser, Phys. Rev. 130, 1441 (1963).

[22]See, for example, John C. Slater Quantum Theory of Molecules and Solids (McGraw-Hill Book Co., Inc., New York, 1963), Vol. I p. 259.

[23]E. Clementi, IBM J. Research Develop. 9, 2 (1965).

[24]Superscripts ±1 will henceforth be used to denote one-electron spin states, and in the diagrams as well.

[25]C. Froese, Can. J. Phys. 41, 1895 (1963).

[26]A. Burgess, Proc. Phys. Soc. (London) 442, 81 (1963). We are grateful to Dr. M. R. C. McDowell for bringing this to our attention.

[27]See, for example, Z. Kopal, Numerical Analysis, (John Wiley & Sons, Inc., New York, 1961).

[28]S. D. Mahanti and N. C. Dutta, unpublished.